Eur. Phys. J. B **19**, 599–606 (2001)

THE EUROPEAN PHYSICAL JOURNAL B

EDP Sciences

Coherent dynamics of magnetoexcitons in semiconductor nanorings

K. Maschke[1,a], T. Meier[2], P. Thomas[2], and S.W. Koch[2]

[1] Institut de Physique Appliquée, École Polytechnique Fédérale, 1015 Lausanne, Switzerland
[2] Department of Physics and Material Sciences Center, Philipps University, Renthof 5, 35032 Marburg, Germany

Received 27 September 2000

Abstract. The coherent dynamics of magnetoexcitons in semiconductor nanorings following pulsed optical excitation is studied. The calculated temporal evolution of the excitonic dipole moment may be understood as a superposition of the relative motion of electrons and holes and a global circular motion associated with the magnetic-field splitting of these states. This dynamics of the electron-hole pairs can be generated either by local optical excitation of an ordered ring or, alternatively, by homogeneous excitation of rings with broken rotational symmetry due to disorder or band tilting.

PACS. 71.35.Cc Intrinsic properties of excitons; optical absorption spectra – 71.70.Ej Spin-orbit coupling, Zeeman and Stark splitting, Jahn-Teller effect – 78.66.-w Optical properties of specific thin films – 42.50.Md Optical transient phenomena: quantum beats, photon echo, free-induction decay, dephasings and revivals, optical nutation, and self-induced transparency

1 Introduction

Most recently it became possible to fabricate ring-like semiconductor nanostructures and to measure some of their optical properties [1–3]. Theoretical studies of excitons and biexcitons in semiconductor nanorings penetrated by a magnetic field have predicted Aharonov-Bohm oscillations [4] in the respective binding energies and oscillator strengths [5–7]. It has been found that for magnetic fluxes $\Phi = (n+1/2)\Phi_0$, where n is an integer and Φ_0 is the flux quantum $\Phi_0 = hc/e$ both, binding energy and oscillator strength pass through a maximum for excitons, and through a minimum for biexcitons. They can in principle be studied using conventional linear and nonlinear optical experiments.

In general, a magnetic flux will lead to a circular motion of both electrons and holes. For optical excitation close to the gap, electrons and holes move in opposite direction, at least in a situation where the Coulomb interaction can be neglected. The corresponding partial electron or hole currents are largest for fluxes $\Phi = (n + 1/4)\Phi_0$ or $\Phi = (n + 3/4)\Phi_0$. For spatially homogeneous optical excitation, the photo-generated carriers follow the well known persistent current scenario [8]. In this situation, the optical excitation would just lead to a transient change of the magnetic moment of the ring.

In the present work we concentrate on the underlying electron-hole dynamics, which can in principle be revealed by local optical pulse excitation. We show that the latter will give rise to a rotating electric dipole moment and, accordingly, to a circularly polarized radiation in the GHz to THz frequency range that is determined by the effective masses of the electrons and holes, the diameter of the ring and the magnetic field strength. The circular motion of the excitonic dipole moment is found to survive in the presence of the Coulomb interaction, provided that the rings are sufficiently small such that their circumference remains of the order of the extension of the relative motion of the correlated electron-hole pair.

We study the dynamics of the dipole moment after optical excitation in the excitonic energy range of a semiconductor nanoring. The model system and the numerical approach are presented in Sections 2 and 3. Results for the noninteracting electron-hole system are given in Section 4 in order to introduce the fundamental physics and notions used in this report. The case of excitonic excitations is discussed in Section 5. In both Sections 4 and 5, we consider local excitation to generate the initial wave packets. This restriction is lifted in Section 6, where we treat the case of homogeneous optical excitation over the entire ring. In this case, the symmetry breaking necessary to form spatially localised wave packets required to reveal the dynamical behaviour, is obtained by introducing spatially inhomogeneous one-particle potentials within the ring. Both, tilting of the bands or energetic site disorder are considered.

It is shown that the dynamical behaviour of the photo-generated excitonic dipole can be described as a superposition of the intra-excitonic wave packet dynamics [9], which is characterized by frequencies in the THz-range, and the dynamics resulting from the magnetic-field splitting of one of the contributing excitonic relative-motion

[a] e-mail: klaus.maschke@epfl.ch

states, corresponding to frequencies in the GHz- to THz-range. This excitonic doublet corresponds to an optically forbidden dipole transition in a totally homogeneous system that becomes, however, allowed when the rotational symmetry is broken either by inhomogeneous excitation or by single-particle potentials inherent to the system itself. The splitting of this state, which is twofold degenerate in the absence of the magnetic field, is periodic in the magnetic flux and vanishes whenever Φ is a multiple of half the flux quantum Φ_0. This effect will be termed as "quantum-confined Zeeman effect". Possible experimental realizations are discussed in the concluding Section 7.

2 The model system

In order to reduce the numerical effort, we restrict our calculations to a two-band model with spinless particles. At first sight, this may seem to be a rather severe approximation. It is, however, directly suitable for the description of some interesting physical situations. In real nanostructures fabricated from III-V-material, the valence-band structure close to the center of the Brillouin zone, and thus the optical resonances near the fundamental edge, consist of energetically well separated levels related to the heavy hole (hh), the light hole (lh) and the split-off (so) valence band. We may then study the situation near the hh-transitions. The latter are still twofold degenerate, but choosing circularly polarized light pulses, only one species of transitions is excited due to the relevant selection rules [10]. This situation can be adequately described within a two-band model. Assuming spinless particles, we disregard spin-flip processes, which would essentially lead to a depopulation of the excited levels and thus to a damping of the signals. In nanostructures, these processes are, however, expected to be slow in comparison with the time scale relevant for the dynamics considered here [11], and thus they may safely be neglected.

We consider a ring consisting of N sites equally spaced with nearest neighbour separation d and with radius $R = Nd/(2\pi)$. The sites at positions n carry two states each with energies ϵ_n^{c} and ϵ_n^{v}, which give the diagonal elements T_{nn}^{c} and T_{nn}^{v} of the Hamiltonian matrix $\mathbf{T}$ in real-space representation. The nondiagonal matrix elements of the Hamiltonian define the coupling of the local basis states to its neighbours. In the presence of a magnetic field and for nearest-neighbour interactions the nonvanishing matrix elements are given by

$$\begin{aligned} T_{n,n+1}^{\mathrm{c}} &= J_{\mathrm{c}} \exp[\mathrm{i}2\pi(\Phi/N)/\Phi_0]\,, \\ T_{n+1,n}^{\mathrm{c}} &= J_{\mathrm{c}} \exp[-\mathrm{i}2\pi(\Phi/N)/\Phi_0] \end{aligned} \tag{1}$$

for the conduction band. Accordingly, the holes in the valence band are described by

$$\begin{aligned} T_{n,n+1}^{\mathrm{v}} &= J_{\mathrm{v}} \exp[-\mathrm{i}2\pi(\Phi/N)/\Phi_0]\,, \\ T_{n+1,n}^{\mathrm{v}} &= J_{\mathrm{v}} \exp[\mathrm{i}2\pi(\Phi/N)/\Phi_0]\,. \end{aligned} \tag{2}$$

Compared to the case without magnetic field, the tight-binding coupling parameters J_{c} and J_{v} are thus multiplied by a phase factor depending on the magnetic flux Φ through the ring [7,12,13]. $\Phi_0 = hc/e$ is the flux quantum.

In the absence of Coulomb interaction the system Hamiltonian reads

$$H_0 = \sum_{nm} T_{nm}^{\mathrm{c}} c_n^+ c_m + \sum_{nm} T_{nm}^{\mathrm{v}} d_n^+ d_m. \tag{3}$$

Here, c_n^+ (c_m) creates (destroys) an electron at site n (m) in the conduction band and d_n^+ (d_m) creates (destroys) a hole at site n (m) in the valence band. The eigenvalues of this Hamiltonian form two bands ($E_\nu(q_i)$, $\nu = c, v$)

$$E_\nu(q_i) = -2J_\nu \cos(q_i d) \tag{4}$$

defined for the wave vectors $q_i, i = 1...N$, where

$$q_i = k_i + \frac{2\pi\Phi}{Nd\Phi_0}, \tag{5}$$

and where k_i are the wave vectors without magnetic field

$$k_i = -\frac{\pi}{d} + \frac{2\pi}{d}\frac{\mathrm{i}}{N}\,. \tag{6}$$

The effective masses at the extrema of the valence and conduction band are then given by

$$m_\nu = \frac{\hbar^2}{2J_\nu d^2}\,, \tag{7}$$

or equivalently

$$m_\nu R^2 \frac{J_\nu}{N^2} = \frac{\hbar^2}{2(2\pi)^2} = \text{const.} \tag{8}$$

The physically relevant parameters are the effective masses m_ν and the radius R of the ring. The parameters J_ν and N are chosen in such a way that i) the dispersions close to the band extrema are representative for realistic semiconductor nanostructures, and ii) that the numerics remains manageable. The calculations discussed below were performed for a ring with radius $R = 11$ nm containing $N = 20$ sites, which corresponds to a site separation $d = 34$ Å. The chosen coupling parameters $J_{\mathrm{c}} = 50$ meV and $J_{\mathrm{v}} = 10$ meV correspond to effective masses close to GaAs values $m_{\mathrm{c}} = 0.064m_0$ and $m_{\mathrm{v}} = 0.32m_0$, where m_0 is the free electron mass. In Section 4 we will also use values $J_{\mathrm{c}} = J_{\mathrm{v}} = 50$ meV for tutorial reasons. A magnetic flux of $\Phi_0/4$ through the ring would require a magnetic field of about 12 T. As shown in the next section, the relevant time scale for the description of the electron-hole dynamics is of the order of 1 to 100 ps, which is well within the coherent excitonic regime of a semiconductor nanostructure. Larger rings would require smaller magnetic fields, but the relevant time scales also become larger, as is shown in Section 5, so that phase-breaking interactions will eventually destroy the coherent dynamics one intents to observe. We therefore believe that the chosen parameters are a good compromise.

Perturbation potentials destroying the rotational symmetry of the ring can easily be introduced in our description by taking site dependent electron and hole energies

$\epsilon_n^{\rm c}$ and $\epsilon_n^{\rm v}$. Disorder in the conduction band is modeled by choosing $\epsilon_n^{\rm c}$ randomly from a Gaussian distribution function $\exp(-(\epsilon_n^{\rm c})^2/2\sigma_{\rm c}^2)$, where $\sigma_{\rm c}$ characterizes the energetic scale of the disorder. Eventually, we will consider also a tilting of the conduction band described by

$$\epsilon_n^{\rm c} = \sigma_t \sin[2(n-1)\pi/N], \tag{9}$$

which corresponds to an additional external potential varying linearly with the y-coordinate in the plane of the ring, given site $n = 1$ lies on the positive x-axis. We will further assume that the disorder potentials for electrons and holes or the respective tilting potentials are correlated, as is often the case in semiconductor nanostructures. We take $\epsilon_n^{\rm v} = (J_{\rm v}/J_{\rm c})\epsilon_n^{\rm c} = (m_{\rm c}/m_{\rm v})\epsilon_n^{\rm c}$, *i.e.*, we weight the potential perturbations inversely with the masses.

The Coulomb interaction is included using the monopole-monopole form

$$H_{\rm C} = \frac{1}{2}\sum_{nm}(c_n^+ c_n - d_n^+ d_n)V_{nm}(c_m^+ c_m - d_m^+ d_m), \tag{10}$$

where

$$V_{nm} = U_0 \frac{d}{\frac{Nd}{\pi}\sin(\frac{\pi}{N}|n-m|) + a_0}\cdot \tag{11}$$

In principle, $H_{\rm C}$ includes the repulsion between electrons and between holes, as well as the electron-hole attraction. In the low-excitation regime considered here, only the latter is relevant. The Coulomb-interaction potential, equation (11), is regularized to avoid the divergence of the exciton binding energy in one dimension. The parameters U_0 and a_0 characterize the strength of the interaction and its spatial variation, respectively. The $\sin(x)$ function in the denominator of equation (11) is needed to describe properly the spatial distance between sites n and m on the ring.

The electron-hole dynamics is of central importance for the here discussed physical phenomena. It is thus essential to treat the relative motion of the Coulomb-correlated electron-hole pair in a proper way. This requirement is satisfied by our present model. It describes correctly the effects of the electron-hole correlation on the optical absorption spectrum where it yields characteristic resonances near the absorption edges, which in a bulk situation would be termed "excitonic bound states" (see also [15]). It is thus able to account for the reduced relative motion of the electron-hole pair on the length scale of the "Bohr radius" and of the diameter of the nanoring. The present model has previously been used to study the center-of-mass and the relative motion of a Coulomb-correlated electron-hole pair in a disordered one-dimensional semiconductor [16].

The coupling of the electronic system to a classical optical electric field is given by

$$H_I = -E(t)P = -E(t)\sum_n(\mu_n d_n c_n + {\mu_n}^* c_n^+ d_n^+), \tag{12}$$

where P is the total optical interband polarization, which is obtained by summing over all microscopic polarizations $\mu_n d_n c_n$, and μ_n are the on-site dipole matrix elements allowing the optical transitions between valence and conduction bands. Homogeneous excitation is obtained with $\mu_n = \mu$, inhomogeneous excitation at site 1 corresponds to the choice $\mu_n = \mu\delta_{1n}$. The electric field pulse is chosen as

$$E(t) = E_0 \frac{1}{\sqrt{\pi}\delta t_{\rm L}} \exp(-{\rm i}\omega_{\rm L} t) \exp\left(-\frac{t^2}{\delta t_L^2}\right)\cdot \tag{13}$$

The time-evolution of the system is then determined by the total Hamiltonian

$$H = H_0 + H_{\rm C} + H_{\rm I}. \tag{14}$$

3 The numerical approach

The time evolution of the interband coherence $p_{lk} = \langle d_l c_k\rangle$ is obtained from the Heisenberg equation together with the total Hamiltonian H. In this work we adopt linear response theory, *i.e.*, we solve the system of differential equations

$$-{\rm i}\partial_t p_{lk} = -\sum_n T_{kn}^{\rm c} p_{ln} - \sum_m T_{ml}^{\rm v} p_{mk} + V_{lk}p_{lk} + E(t)\mu_l^*\delta_{lk}. \tag{15}$$

The electron and hole densities $n_{ll}^{\rm c}$ and $n_{ll}^{\rm v}$ can be obtained from the conservation laws [14] valid in the linear response regime

$$\begin{aligned} n_{ll}^{\rm c} &= \sum_k p_{kl}p_{kl}^* \\ n_{ll}^{\rm v} &= \sum_k p_{lk}p_{lk}^*. \end{aligned} \tag{16}$$

The electron and hole dipole moments $\mathbf{d}^{\rm c}$ and $\mathbf{d}^{\rm v}$ defined with respect to the center of the ring are given by

$$\begin{aligned} d_x^\nu &= \pm e\sum_l n_{ll}^\nu R\cos\phi_l \\ d_y^\nu &= \pm e\sum_l n_{ll}^\nu R\sin\phi_l, \end{aligned} \tag{17}$$

where $\phi_l = 2\pi(l-1)/N$ defines the angular position of site l. The signs depend on the charge of the particle in band ν, negative signs correspond to electrons, positive signs to holes. The total electron-hole dipole moment $\mathbf{d}$ is

$$\mathbf{d} = \mathbf{d}^{\rm c} + \mathbf{d}^{\rm v}. \tag{18}$$

The optical ε_2-spectra are calculated by Fourier transforming the optical interband polarization $p_{lk}(t)$ corresponding to a short pulse ($\delta t_{\rm L} = 0.1$ ps) excitation with central frequency $\omega_{\rm L}$ close to the lowest transition. The spectra are calculated assuming a polarization decay time $T_2 = 50$ ps, while we use $T_2 \to \infty$ for the calculation of the coherent dynamics.

The dynamical motion of the dipole may be considered as a source of electromagnetic radiation. The associated

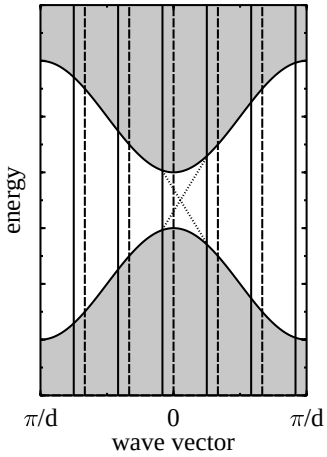

Fig. 1. Band structure of a ring composed from $N = 6$ sites for equal electron and hole masses. The vertical dashed lines indicate direct transitions at wave vectors k_m, the vertical solid lines those at wave vectors $q_m = k_m + \frac{1}{4}\frac{2\pi}{Nd}$ shifted by the magnetic flux $\Phi = \Phi_0/4$. Dotted lines indicate the lowest indirect transitions for inhomogeneous excitation.

electric field is obtained from the second time derivative of the dipole moment, which constitutes the source term in Maxwell's equations. The corresponding polarization angle is determined by

$$\alpha = \arctan \frac{\mathrm{d}^2 \mathrm{d}_y/\mathrm{d}t^2}{\mathrm{d}^2 \mathrm{d}_x/\mathrm{d}t^2} \,. \tag{19}$$

4 Local excitation of the noninteracting system

In order to elucidate the underlying basic physical mechanism, we consider first the case $U_0 = 0$ and $J_\mathrm{c} = J_\mathrm{v} = 50$ meV. Figure 1 shows the valence and conduction bands as well as the relevant optical transitions for $N = 6$. The wave vectors k_m for the magnetic-field-free case $\Phi = 0$ are denoted by vertical dashed lines, those for $\Phi = \Phi_0/4$ by solid lines. For $\Phi = 0$ there are two twofold degenerate optical dipole transitions (at $k = \pm\pi/3d$ and $k = \pm 2\pi/3d$), and two nondegenerate transitions (at $k = 0$ and $k = \pi/d$). For $\Phi = \Phi_0/4$ the degeneracies are lifted and the spectrum consists of 6 lines. It can easily be seen that one would obtain three twofold degenerate transitions for $\Phi = \Phi_0/2$.

The optical ε_2-spectrum, which corresponds to the linear absorption spectrum, is shown in Figure 2 for $N = 20$. The lines pointing downward show the 11 transitions for $\Phi = 0$, the upward pointing lines show the 20 nondegenerate transitions for $\Phi = \Phi_0/4$. Note that the amplitudes are determined by the degeneracies of the corresponding transitions.

We concentrate on the transitions close to the fundamental gap. As can be seen in Figure 2, the two lowest transitions in the spectrum for $\Phi = \Phi_0/4$ are strongly dependent on the magnetic flux. They merge for $\Phi \to \Phi_0/2$.

In the following we assume inhomogeneous excitation, where the optical excitation takes place at a single site

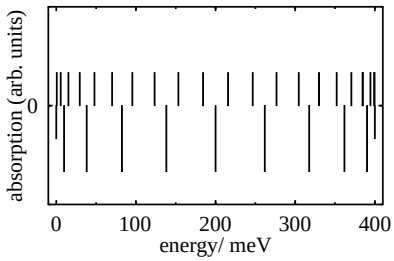

Fig. 2. Optical spectrum due to direct transitions for a homogeneous ring with $N = 20$ sites, equal electron and hole masses, $J_\mathrm{c} = J_\mathrm{v} = 50$ meV, and without Coulomb interaction, $U_0 = 0$. Pointing downwards: no magnetic flux. Pointing upwards: $\Phi = \Phi_0/4$.

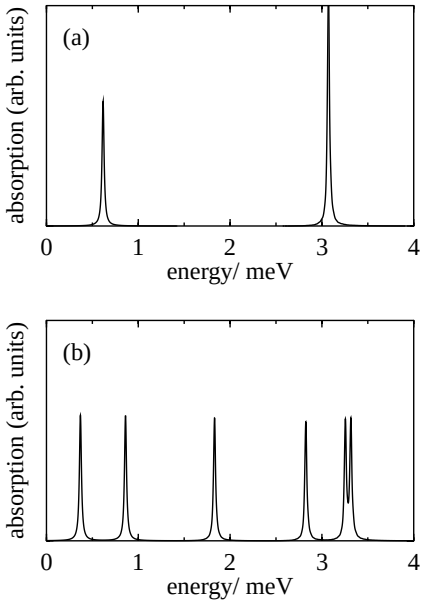

Fig. 3. Optical spectrum for the homogeneous ring with $N = 20$ close to the fundamental gap, no Coulomb interaction, $U_0 = 0$, and local excitation at site $n = 1$. The magnetic flux is $\Phi = \Phi_0/4$. (a) Equal electron and hole masses $J_\mathrm{c} = J_\mathrm{v} = 50$ meV. The higher energy peak is due to the twofold degenerate indirect transitions indicated by dotted lines in Figure 1. (b) Different electron and hole masses $J_\mathrm{c} = 50$ meV, $J_\mathrm{v} = 10$ meV. The degeneracy is lifted.

only ($n = 1$, on the positive x-axis). In this situation additional transitions become allowed which are not shown in Figure 2. In order to resolve the spectrum for this situation, we present an enlarged view of the low-energy transitions in Figures 3 and 4. Here and in the following the energy zero corresponds to the lowest transition energy of the perfect noninteracting system for $\Phi = 0$. In the spectrum for $\Phi = \Phi_0/4$, Figure 3a, we find two absorption lines spaced by about 2.5 meV. The lower peak corresponds to the shifted $k = 0$ transition, the higher one is associated with the first indirect transitions, which are twofold degenerate in the case of equal electron and hole masses (see dotted lines in Fig. 1).

The optical pulse has an average excitation energy ω_L close to the fundamental gap and a temporal width

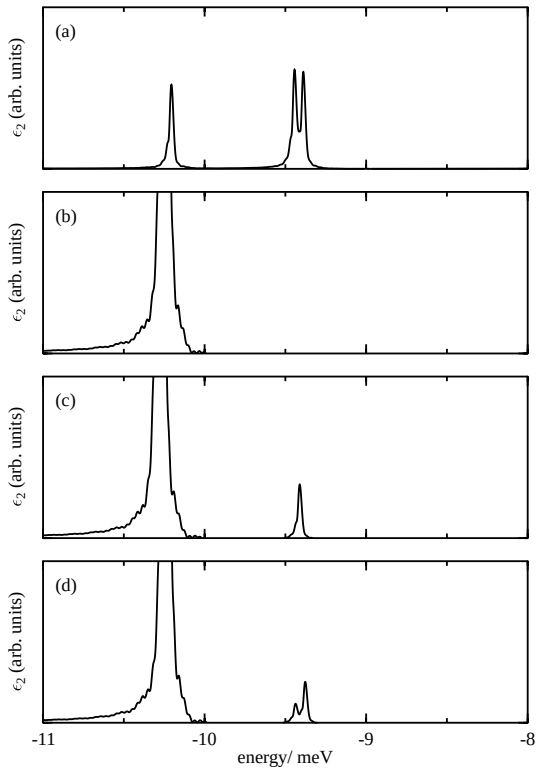

Fig. 4. Optical spectrum close to the fundamental gap for the ring with $N = 20$ sites for different electron and hole masses, $J_c = 50$ meV, $J_v = 10$ meV, with Coulomb interaction $U_0 = 16.5$ meV. (a) Homogeneous ring, local excitation at site $n = 1$ and magnetic flux $\Phi = \Phi_0/4$. (b) Homogeneous ring, homogeneous excitation, magnetic flux $\Phi = 0$. The peak is the lowest excitonic resonance. (c) Tilted bandstructure, $\sigma_t = 0.2$ meV, homogeneous excitation, magnetic flux $\Phi = 0$. In addition to the lowest excitonic resonance the next higher excitonic states become optically allowed. (d) Same as c), but with magnetic flux $\Phi = \Phi_0/4$. The second resonance is splitted.

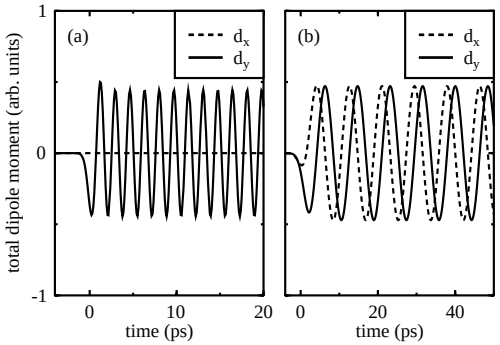

Fig. 5. Total dipole moment $\mathbf{d}(t) = (d_x(t), d_y(t))$ as a function of time. (a) Equal electron and hole masses, *cf.* Figure 3a. (b) Different masses, *cf.* Figure 3b.

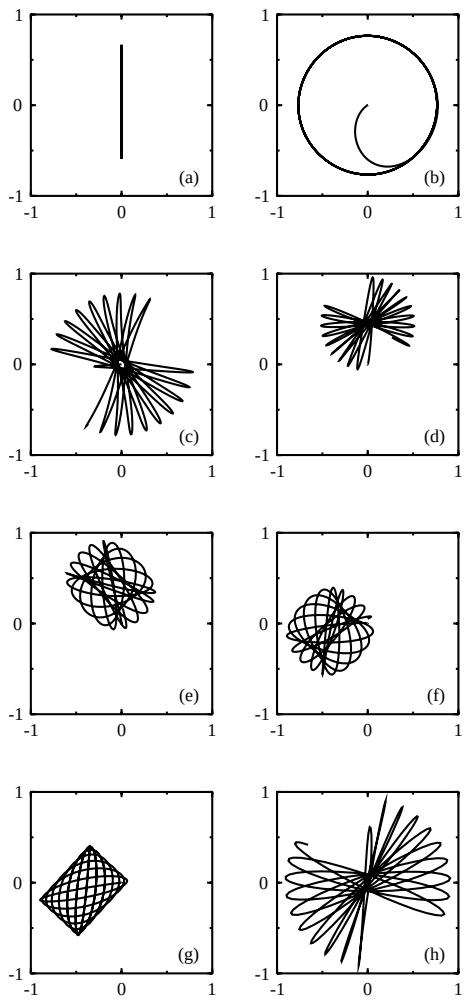

Fig. 6. Trace of the total dipole moment $\mathbf{d}(t) = (d_x(t), d_y(t))$ (a – g) and of the second time derivative of the total dipole moment (h) for $\Phi = \Phi_0/4$. Vertical axes: y-direction, horizontal axes: x-direction. (a) Equal electron and hole masses, inhomogeneous excitation at site $n = 1$ of the homogeneous ring, $U_0 = 0$, *cf.* Figure 3a. The polarization is linear. (b) Different masses, inhomogeneous excitation at site $n = 1$ of the homogeneous ring, $U_0 = 0$, *cf.* Figure 3b. The polarization is circular. (c) Inhomogeneous excitation at site $n = 1$ of the homogeneous ring, $U_0 = 16.5$ meV, *cf.* Figure 4a. (d) Same as (c), but homogeneous excitation of a ring with tilted band structure, $\sigma_t = 0.1$ meV, *cf.* Figure 4d. Note the qualitative similarity with Figure 6c. (e) Homogeneous excitation of the ring with tilted bandstructure and disorder, $\sigma_c = \sigma_t = 0.1$ meV, $U_0 = 16.5$ meV. (f) Homogeneous excitation of the ring with disorder and without band tilting, $\sigma_c = 0.1$ meV, $\sigma_t = 0$, $U_0 = 16.5$ meV. (g) Same as (f), but without magnetic flux, $\Phi = 0$. (h) Second time derivative of the total dipole moment for the situation of Figure 6d.

of $\delta t_L = 1$ ps. The resulting total dipole moment $\mathbf{d}$ of the photo-generated electron-hole pair is shown in Figure 5a, where the x-component $d_x(t)$ and the y-component $d_y(t)$ are shown as a function of time. Electron and hole start at site $n = 1$ and move into opposite directions with equal velocities, since their masses are equal. Thus $d_x(t)$ remains zero while $d_y(t)$ oscillates. The trace $d_y(d_x)$ shows the linear polarization of this motion (see Fig. 6a). The oscillation frequency of $d_y(t)$ is determined by the energetic separation of the involved transitions. For small energetic pulse widths like in our calculation only the two lowest transitions contribute and the motion is purely sinusoidal.

In realistic semiconductors electron and hole masses will be different. In this case the situation may change

considerably. Figure 3b shows the spectrum close to the gap for a ring with $J_c = 50$ meV and $J_v = 10$ meV for excitation at site $n = 1$ and $\Phi = \Phi_0/4$. The peak with lowest energy corresponds again to the direct transition between the lowest electron state and the highest hole state, which would correspond to the $k = 0$ transition in the absence of the magnetic flux. The second peak, however, is now due to the indirect transition between the same electron state and the next hole state. Both transitions are nondegenerate because of the different masses. As for energetically narrow pulses only a single electron k-state contributes, the electron density is homogeneously distributed over the ring after the light pulse, yielding $\mathbf{d}^c = 0$. On the other hand, the two contributing hole states form a wave packet that moves around the ring with a velocity given by the energetic phase factors of the two states involved. This leads to a circularly polarized motion of the total dipole moment $\mathbf{d}(t)$ as seen in Figures 5b and 6b, where both $d_x(t)$ and $d_y(t)$ as well as the trace $d_y(d_x)$ are shown.

5 Local excitation of the interacting system

Coulomb interaction between electron and hole is expected to be important for the wave packet dynamics. In the following we assume $U_0 = 16.5$ meV, which corresponds to a binding energy of about 10 meV [15].

Magnetic field effects in the low-energy excitations can only be expected if the corresponding electron-hole pairs are not too tightly bound, or – in other words – if the excitonic Bohr radius remains comparable with the ring circumference. As already mentioned above, small rings are required in any case, since the coherent dynamics can only take place on a time scale smaller than the dephasing time. For given effective masses, the differences in energy leading to the circular motion and thus the time scale of the circular dynamics, depend solely on the ring radius R and increase as $1/R^2$ with decreasing R. In particular, the energetic distances do not depend on the number of sites N nor on the site separation d or the coupling parameters J_ν for fixed masses and radius.

Similar to the previous section, we first consider a homogeneous ring and local excitation at site $n = 1$. The lowest transitions are shown in Figure 4a. We see a single peak near –10 meV and a split peak near −9.4 meV. Comparison with the absorption spectrum for homogeneous excitation (Fig. 4b–d) shows that this doublet originates from a higher twofold degenerate (for $\Phi = 0$) excitonic bound state with odd parity, which is optically forbidden for homogeneous excitation. This transition becomes, however, allowed if the symmetry is broken as *e.g.* under local excitation conditions, where the circular symmetry of the system is perturbed by the local excitation itself. Alternatively, the symmetry may be broken by a perturbing one-particle potential. This is also evident from Figures 4c and 4d, which show the absorption spectra for homogeneous excitation for $\Phi = 0$ and for $\Phi = \Phi_0/4$, but where now additional band-tilting potentials $\epsilon_n^c = \sigma_t \sin[2(n-1)\pi/N]$ and $\epsilon_n^v = (J_c/J_v)\sigma_t \sin[2(n-1)\pi/N]$ are added to the conduction and valence band site energies, respectively. In this case, the symmetry is broken by the additional potentials, and the optical transition into these states becomes allowed even under homogeneous excitation conditions.

The doublet splitting in Figure 4a is due to the magnetic flux, as can also been seen in Figure 4d. This splitting is periodic with period $\Phi_0/2$. This effect could be called "quantum confined Zeeman effect". The period halfing is due to the fact that the two peaks cross at $\Phi = \Phi_0/2$.

Similar to the situation treated in the previous section, the optical excitation of the doublet structure leads to electron and hole wave packets moving in opposite directions, but now with different velocities. The time scale of the rotation is determined by the small splitting of the doublet. The rotation frequency is thus considerably smaller than the superimposed linear oscillation which is due to the contribution of the lowest excitonic transition, and which scales with the energetic distance between the first absorption peak and the doublet. This explains the rosette-like trace of the total dipole moment shown in Figure 6c. With our parameters, the circular component has a period of 100 ps, while that of the linear component has a period of the order of 5 ps.

6 Homogeneous excitation of the inhomogeneous system

6.1 Band tilting

As already mentioned in the previous Section 5, spectra and dynamical behaviour similar to Figures 4a and 6c can be obtained also under homogeneous optical excitation conditions, provided that the rotational symmetry is broken by an additional one-particle potential. This situation will be investigated in the present section. We consider the sinusoidal perturbation potential equation (9), $\epsilon_n^c = \sigma_t \sin[2(n-1)\pi/N]$ and $\epsilon_n^v = (J_c/J_v)\epsilon_n^c$, applied to the conduction and valence band site energies, respectively.

Figures 4b, 4c and 4d show the spectra close to the absorption edge for $\Phi = 0$ and $\sigma_t = 0$, $\Phi = 0$ and $\sigma_t = 0.2$ meV, as well as for $\Phi = \Phi_0/4$ and $\sigma_t = 0.2$ meV, respectively. The dynamics of the total dipole moment is shown in Figure 6d for $\sigma_t = 0.1$ meV. It closely resembles that of Figure 6c for the perfect ring with single-site excitation. The additional stationary dipole moment seen in Figure 6d is caused by the tilting of the valence and conduction bands. The stationary dipole moment increases with the amplitude of the sinusoidal potential, whereas the amplitude of the dynamic motion decreases. The latter feature is due to the fact that the excitonic wave function becomes more confined for larger amplitudes σ_t and finally localizes in the region where the differences between the site energies are smallest.

The source term in Maxwell's equations, which is given by the second time derivative of the dipole moment, is shown in Figure 6h. It essentially reflects the dynamical part of the total dipole moment shown in Figure 6d.

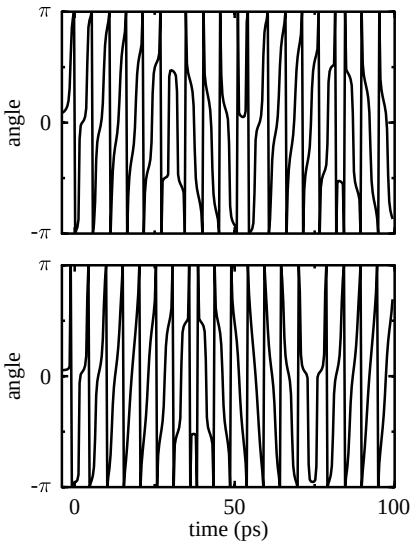

Fig. 7. Polarization angle α, see equation (19), as a function of time for homogeneous excitation of the disordered ring. Upper panel: With magnetic flux $\Phi = \Phi_0/4$, *cf.* Figure 6f. There is no time reversal. The circular character is clearly seen. Lower panel: Without magnetic flux, *cf.* Figure 6g. Two perfect time reversals can be identified.

6.2 Disorder

Similar effects as discussed above may be expected for a disorder potential, which again will break the circular symmetry of the ring, thus rendering transitions into higher excitonic states allowed. A random potential, however, leads to a somewhat more complicated trace of the total dipole, as shown in Figure 6e, where in addition to the previously used sinusoidal potential we have added a random potential with $\sigma_c = \sigma_t = 0.1$ meV. Again a stationary dipole is found which results from a fluctuation of the local band gap, but it now points into a slightly different direction. Figure 6f shows the situation without sinusoidal potential. In this case the stationary dipole has changed its direction, which is now solely determined by the disorder potential. The dynamical part still looks very similar. The magnetic flux $\Phi = \Phi_0/4$ leads to a circular component in the dynamical trace, as can be seen in the upper panel of Figure 7, where the polarization angle α defined in equation (19) is shown. The motion is in general not periodic. In fact, a periodic evolution would require that the energies involved have rational ratios. The dynamics of the total dipole moment in the absence of the magnetic field is shown in Figure 6g, the corresponding angle α is presented in the lower panel of Figure 7. It is seen that the motion periodically changes its direction, and there is no circular component on the temporal average.

7 Conclusions

We have shown that excitonic wave packets can be generated in semiconductor nanorings penetrated by a magnetic flux either by local excitation of a homogeneous ring or by homogeneous excitation of an inhomogeneous ring. The resulting dynamics of the electric dipole moment can be described as a superposition of a nearly linear oscillation and a circular motion, where the latter is due to the magnetic field. The expected absolute magnitude of the dipole moment is of the order of or smaller than the diameter of the ring times the elementary charge. It depends on the excitation intensity, which, however, has to be kept small enough in order to avoid dephasing due to Coulomb scattering.

Experimentally, the dipole motion could be detected by measuring the corresponding electromagnetic field, which will follow the underlying polarization pattern. Alternatively, one could use also pump-probe or four-wave-mixing to observe the predicted effects, as has been successfully done in the case of Bloch oscillations in biased semiconductor superlattices [17].

In order to obtain observable signals it will probably be necessary to perform the experiments on ensembles of rings. The excitation has then to be homogeneous over the entire ensemble, and a gradient of composition or strain should be applied to produce the sinusoidal symmetry breaking potential.

Disorder will always be present in real samples. Our results show, however, that it does not disturb the dynamics of a single ring severely. For an ensemble of many nanorings, the disorder induced changes are expected to cancel out at times longer than the pulse duration. As an alternative to such an ensemble one might fabricate a quantum well with closely spaced holes of diameters in the 10 to 100 nm range. This arrangement should also facilitate the creation of a band gap gradient over the sample. Although the different rings have then slightly different optical gaps, the dynamics of the dipole moment is identical for all rings.

We profited from stimulating discussions with R.A. Römer and Guido Burmeister. Support in the initial stage of this work by Thomas Lemm is also acknowledged. PT acknowledges the hospitality of the Institut de Physique Appliquée, École Polytechnique Fédérale, Lausanne. This work was partly supported by the Swiss National Science Foundation under Grant No. 20-58972.99, by the Max-Planck Research prize of the Humboldt and Max-Planck Societies, by the Deutsche Forschungsgemeinschaft (DFG) through the Sonderforschungsbereich 383 and the Quantenkohärenz Schwerpunkt, and by the Leibniz prize.

References

1. A. Lorke, R.J. Luyken, A.O. Govorov, J.P. Kotthaus, J.M. Garcia, P.M. Petroff, Phys. Rev. Lett. **84**, 2223 (2000).
2. R.J. Warburton, C. Schäflein, D. Haft, F. Bickel, A. Lorke, K. Karrai, J.M. Garcia, W. Schoenfeld, P.M. Petroff, Nature **405**, 926 (2000).
3. H. Pettersson, R.J. Warburton, A. Lorke, K. Karrai, J.P. Kotthaus, J.M. Garcia, P.M. Petroff, Physica E **6**, 510 (2000).
4. Y. Aharonov, D. Bohm, Phys. Rev. **115**, 485 (1959).
5. A.V. Chaplik, Pisma Zh. Exsp. Teor. Fiz. [JETP Lett. **62**, 900 (1995)].

6. R.A. Römer, M.E. Raikh, Phys. Rev. B **62**, 7045 (2000); Phys. Stat. Sol. (b) **221**, 535 (2000).
7. T. Meier, P. Thomas, S.W. Koch, Eur. Phys. J. B, submitted.
8. M. Büttiker, Y. Imry, R. Landauer, Phys. Lett. A **96**, 365 (1983).
9. J. Feldmann, T. Meier, G. von Plessen, M. Koch, E.O. Göbel, P. Thomas, G. Bacher, C. Hartmann, H. Schweizer, W. Schäfer, H. Nickel, Phys. Rev. Lett. B **70**, 3027 (1993); F. Jahnke, M. Koch, T. Meier, J. Feldmann, W. Schäfer, P. Thomas, S.W. Koch, E.O. Göbel, H. Nickel, Phys. Rev. B **50**, 8114 (1994).
10. C. Sieh, T. Meier, F. Jahnke, A. Knorr, S.W. Koch, P. Brick, M. Hübner, C. Ell, J. Prineas, G. Khitrova, H.M. Gibbs, Phys. Rev. Lett. **82**, 3112 (1999); T. Meier, S.W. Koch, M. Phillips, H. Wang, Phys. Rev. B **62**, 12605 (2000).
11. T. Armand, X. Marie, P. Le Jeune, M. Brousseau, D. Robart, J. Barrau, Phys. Rev. Lett. **78**, 1355 (1997).
12. N. Byers, C.N. Yang, Phys. Rev. Lett. **7**, 46 (1961).
13. F. Bloch, Phys. Rev. B **2**, 109 (1970).
14. K. Victor, V.M. Axt, A. Stahl, Phys. Rev. B **51**, 14164 (1995).
15. The terminology may be somewhat misleading. The notion of "binding energy", "exciton" and "Bohr radius" should be used with some care. In a ring all states are discrete, *i.e.* they are all bound states with a finite extension. In addition, the form of the Coulomb interaction matrix element in a nanoring takes care of the ring geometry, and it differs therefore from that in a one-dimensional chain. Nevertheless we will use these notions, since – similar to the bulk situation – the interaction lowers the transition energies at the absorption edge with respect to the noninteracting case. In the here adopted terminology, "binding energy" just means the energetic difference between the lowest absorption peaks calculated with and without interaction.
16. D. Brinkmann, J.E. Golup, S.W. Koch, P. Thomas, K. Maschke, I. Varga, Eur. Phys. J. B **10**, 145 (1999).
17. J. Feldmann, K. Leo, J. Shah, D.A.B. Miller, J.E. Cunningham, T. Meier, G. von Plessen, A. Schulze, P. Thomas, S. Schmitt-Rink, Phys. Rev. B **46**, 7252 (1992); T. Meier, G. von Plessen, P. Thomas, S.W. Koch, Phys. Rev. Letters **73**, 902 (1994); T. Meier, G. von Plessen, P. Thomas, S.W. Koch, Phys. Rev. B **51**, 14490 (1995); V.G. Lyssenko, G. Valusis, F. Löser, T. Hasche, K. Leo, M.M. Dignam, K. Köhler, Phys. Rev. Lett. **79**, 301 (1997).